COO-1198-473

SOME ASPECTS OF PHASE TRANSFORMATION IN NEAR-EQUIATOMIC NIOBIUM-RUTHENIUM ALLOYS*

Nb - Ru

by

BIJOY KISHORE DAS

Department of Mining, Metallurgy, and Petroleum Engineering

and Materials Research Laboratory

University of Illinois, Urbana, Illinois

August, 1967

*This research was supported in part by the U. S. Atomic Energy Commission under Contract AT(11-1)-1198 (Report No. COO-1198-473). This report is based on a thesis submitted in partial fulfillment of the requirements for the degree of Master of Science in Metallurgical Engineering in the Graduate College of the University of Illinois, 1967.

DISCLAIMER

ACKNOWLEDGEMENT

The author gratefully acknowledges the continuous guidance and encouragement of Professor D. S. Lieberman throughout this investigation. The author also wishes to thank Mr. R. Hoffman for his assistance in preparation of specimens and Mr. M. A. Schmerling for his assistance in all phases of this work.

The author acknowledges the financial support from the U. S. Atomic Energy Commission under the Contract AT(11-1)-1198.

TABLE OF CONTENTS

		PAGE
I.	INTRODUCTION	1
II.	EXPERIMENTAL TECHNIQUES	
	A. PREPARATION OF SPECIMENS	3
	B. ELECTRICAL RESISTANCE MEASUREMENTS	5
	C. METALLOGRAPHY AND HOT STAGE OPTICAL MICROSCOPY	6
	D. MAGNETIC SUSCEPTIBILITY MEASUREMENTS	7
	E. X-RAY MEASUREMENTS	8
III.	RESULTS AND DISCUSSION	9
IV.	CONCLUSIONS	19
V.	REFERENCES	60
VI.	APPENDIX	61

I. INTRODUCTION

Martensitic phase transformations in intermetallic compounds have been studied because of important changes in some of the physical properties accompanying the transformations and because of the interest in the crystallography of such transformations.[1] The present study was undertaken to investigate whether such a transformation occurs in near-equiatomic Nb-Ru alloys, as suggested by earlier workers.[2,3,4,5]

Greenfield and Beck,[2] who first investigated the Nb-Ru system, reported from room temperature X-ray measurements that alloys between 48 and 49 at.% Ru have a body-centered tetragonal structure when quenched from 1200°C. However they also reported that an alloy containing 32 at.% Ru, when treated the same way, has a b.c.c. or possibly a CsCl structure (very weak super lattice lines resulted because of small difference in scattering powers of Nb and Ru) at room temperature. A. E. Dwight[3] later reported parallel markings on a 47.6 at.% Ru specimen quenched from 1200°C to room temperature, the room temperature structure of the alloy being b.c.t. with a c/a of 1.12. Later work by Raub and coworkers[4] confirmed the presence of a body-centered tetragonal phase between 41 and 46.5 at.% Ru on quenching from 1200°C to room temperature. They also reported alloys having compositions between 47 and 58 at.% Ru to have a face-centered orthorhombic structure on quenching from 1200°C to room temperature. Kaufmann and coworkers[5] constructed the Nb-Ru phase diagram (Figure 1) using X-ray, metallogra-

phic and other techniques. According to them maximum solid solubility of Ru in Nb is 58 at.% at room temperature and there are a maxima and a minima in solidus at 1870°C and 40 at.% Ru, and 1942°C and 50 at.% Ru respectively. They also reported that at room temperature, alloys containing between 40 at.% Ru and 58 at.% Ru have a body-centered tetragonal crystal structure; parallel markings were observed metallographically.

On basis of experience in other CsCl type intermediate phases such as AuCd, AuMn, CuZn, etc., which are known to undergo martensitic transformations,[1] the above mentioned observations suggested that near-equiatomic Nb-Ru alloys transform martensitically from a CsCl type parent phase to a phase having lower symmetry. In the present study metallographic, magnetic, resistometric, and X-ray techniques have been used to determine whether a martensitic phase transition occurs in these alloys, and, if so, to investigate the mechanism of such a transformation and the structure of the product phase.

II. EXPERIMENTAL TECHNIQUES

A. Preparation of Specimens

Niobium metal of 99.95 wt.% purity, supplied by Kawecki Chemical Co. in -60 mesh powder form, and ruthenium metal of 99.98 wt.% purity, supplied by Engelhard Industries in -80 mesh powder form, were used to grow all specimens. It was found that arc-melted buttons of Nb-Ru alloys containing nearly 50 at.% Ru are very brittle and hence could not be swaged into rods suitable for resistance measurements. Attempts to melt the alloys in an arc furnace and cast them in a rod form using a suitably designed hearth failed because the molten metal could not flow very far before freezing in the water cooled hearth.

The method finally adopted was zone melting of powder compacts of nominal compositions which were formed by mixing Nb and Ru powders thoroughly and pressing them into 1/8"x1/8"x2" rods in a die (Figure 2) using a hydraulic press at a pressure of 30,000 psi. The density of the compacts on the average was 61% of the theoretical density. The zone melting of the compacts was done in an MRC electron beam zone refiner operating at a pressure of less than 10^{-6} torr. One end of the compact was welded onto a Nb rod (99.95 wt.% pure); the other end of the compact was at first welded onto another Nb rod, and the compact was melted by passing a liquid zone through it. However, it was later found that use of a powder compact in place of a Nb rod at the end, at which the liquid zone was first struck, gave a more stable zone. Further,

the power needed to melt the alloy after alloying took place was much less since alloys melt at a considerably lower temperature than either Nb or Ru, which melt at 2468°C and 2300°C respectively.[5]

The phase diagram of the Nb-Ru system (Figure 1) shows that the separation between solidus and liquidus between 40 and 50 at.% Ru is very small and hence specimens of compositions in this range prepared by zone melting are expected to have very small composition gradients along their lengths. To minimize any such gradients in these alloys and in alloys of composition outside this range, zone leveling was employed. Three passes both up and down the specimen in each direction were made. The average compositions of the three alloys prepared as determined by chemical analysis* are listed in Table 1.

Table 1. Average Compositions of the Alloys

Alloy #	Nominal Composition at.% Ru	Average Composition at.% Ru
1	45.0	45.8
2	50.0	51.1
3	55.0	55.8

Table 2 shows the compositions of four samples of nearly equal length, made by breaking the rod-like specimen, as arranged from one end.

---

*The technique used for chemical analysis was colorimetry based on absorption of 4650Å radiation by K-ruthenate in 2 molar KOH solution.

Table 2. Composition Gradient in the Specimen

Alloy #	Compositions at.% Ru
2	51.0, 51.3, 51.3, 50.9
3	55.7, 55.9, 56.3, 55.4

It was concluded that there was no composition gradient within the limits of accuracy of the technique used for chemical analysis, which was ± 1 at.% Ru.

B. Electrical Resistance Measurements

To explore the possibility of a martensitic transformation in the prepared alloys, electrical resistance* was measured up to 1300°C by passing a direct current of 1.019 amps. (as determined by the potential drop across an 1 ohm standard resistor) through a specimen and measuring the potential drop across it with a Rubicon potentiometer capable of measuring 5 microvolts. The current through the specimen was controlled within ± 0.001 amp. using a feed back mechanism shown in Figure 3. The four 20 mil Pt wires used for current and potential leads and the two Pt, Pt-10% Rh thermocouples were welded to the specimen as shown in Figure 4; all the wires were insulated with alumina beads. The specimen was suspended inside an alumina tube with the

*Since the specimens used for resistance measurements were not uniform in diameter and since resistance changes alone are sufficient to indicate the transformations, no attempt was made to evaluate the resistivity of the alloys as a function of temperature.

lead wires and heated by induction using a tantalum susceptor, which was insulated from the induction coil by another alumina tube (Figure 4). Since the alloys used are very easily oxidized, heating was done under a pressure of 5×10^{-6} torr or less. Two alumina disc reflectors one at the top of the inner alumina tube and the other at the bottom of the same tube were used to reduce the temperature gradient along the length of the specimen from 25°C/inch to 5°C/inch. To cancel out any thermal e.m.f., potential drops across the specimen when current was flowing through it in two opposite directions were measured and resistance of the specimen was computed by taking the average of the two.

In order to find out any possible effects of high frequency induction heating of the specimen on its resistance measurements and to check this technique, resistivity of Ta (99.95 wt.% pure) was measured up to 1100°C using a 2" long 1/8" diameter Ta rod. The data obtained agree fairly well with that of R. P. Tye[6] (Figure 5).

C. Metallography and Hot Stage Optical Microscopy

Small specimens 1/16" thick and 1/8" diameter were cut from the rod-like specimens using a spark cutter. They were then wet polished at room temperature through 4/0 grade paper. Due to the extreme hardness of the specimens, a satisfactory final polish could not be obtained using alumina powders. However, 3 micron and 1 micron diamond pastes gave a good final polished

surface. Satisfactory etching was obtained by etching electrolytically with a solution of 1.25% HF and 5% H_2SO_4 in methanol at a voltage of 10-15 volts for 1 minute.

For hot stage microscopy, a Leitz heating stage was used. The specimen was spot welded to the two wires of a Pt, Pt-10% Rh thermocouple and heated to 1600°C under a pressure of less than 10^{-5} torr using a tantalum heater of the design shown in Figure 6. Some fogging of the heating stage was observed at about 1300°C. The temperature of the specimen was controlled by a temperature controller and the specimen could be heated or cooled manually; heating and cooling rates up to 4000°C/min. could be obtained.

D. Magnetic Susceptibility Measurements

Determination of the variation of magnetic susceptibility with temperature for both bulk and powder specimens was necessary as pointed out later. Bulk specimens were prepared by breaking the rod-like specimens into 4 or 5 pieces each about 1/2" long. They were then sealed off in a quartz capsule at a pressure of less than 10^{-6} torr and the capsule was then suspended inside a Varian superconducting magnet solenoid with a maximum field of 40 kilogauss. A molybdenum wound furnace was used to heat the capsule to 1000°C and the change in the weight of the capsule was measured with an analytic pan balance as the capsule was heated and cooled. Powders were then prepared from the pieces used for the bulk measurements

in a porcelain mortar and pestle to avoid contamination by any ferromagnetic material. Magnetic susceptibility of the powders was measured by the method outlined for bulk specimens.

The force exerted on the capsule minus the quartz correction (i.e., the force exerted on a dummy quartz capsule with no specimen inside) is proportional to the magnetic susceptibility as given by the relation,[7]

$$F = 1/2\ m\chi d/dx(H^2)$$

where F = force on the specimen after quartz correction,

m = mass of the specimen,

χ = magnetic susceptibility of the specimen, and

H = applied magnetic field.

E. X-ray Measurements

Powder patterns of all the alloys were taken at room temperature with a 5.73 cm. diameter Phillips camera using powders (-325 mesh) prepared by powdering the mid portion of each specimen with mortar and pestle. The powders were put on the surface of a 0.1 mm. diameter glass fibre with some vaseline and the fibre was then fixed onto the camera. Filtered Cu radiation was used and the X-ray tube was operated at 20 kv. and 30 ma. with an exposure time of 2 hours.

III. RESULTS AND DISCUSSION

In case of all the three alloys, the departure of the resistance vs. temperature curves from linearity on both cooling and heating (Figures 7-9) was associated with changes in microstructure (see below) and hence phase transformations. In all three cases, although the transformation regions extend over several hundred degrees, the resistance vs. temperature curves show no hysteresis within the errors of this exploratory experiment -- $\pm 10^{\circ}C$ -- which are primarily due to the temperature gradient in the specimen. Different heating rates (from $50^{\circ}C$/hr to $300^{\circ}C$/hr) produce little effect on the details of resistance changes in any of the specimens. In keeping with similar changes in other alloy systems, the temperature at which the high temperature parent phase begins to transform on cooling will be called M_s, and the temperature at which the low temperature product phase begins to transform on heating will be called A_s, even though the phases bear no resemblance to the "martensite" and "austenite" in the iron base alloys after which they are named; M_f and A_f are similarily employed for completion temperatures respectively.

M_s and M_f for alloy 1 (45.8 at.% Ru) are $525^{\circ}C$ and $150^{\circ}C$ respectively (Figure 7). The slope of the resistance vs. temperature curve remains essentially constant during the transformation. Since no hysteresis is observed within experimental error, $A_s = M_f$ and $A_f = M_s$; the resistance increase during the transformation is

17%. In case of alloy 2 (51.1 at.% Ru) on cooling the transformation starts at 900°C and the resistance of the alloy increases with decreasing temperature to 700°C, below which it continues to decrease linearily (Figure 8). However in contrast to Figure 7 there is a definite change in the slope of the resistance vs. temperature curve by a factor of two at about 790°C, indicating a more complex phenomenon than in Figure 7. It is interesting to note that even the complex behavior shown in Figure 8 shows no hysteresis and the changes in slope of the resistance vs. temperature curve occur at the same temperatures on both cooling and heating. Alloy 3 (55.8 at.% Ru) shows an A_s of 950°C (Figure 9). The data in this case show more scatter since the change in resistance for a 20°C change in temperature (the general temperature interval of measurements) is much less than that in case of the other two alloys and is of the order of the accuracy of resistance measurement, i.e., 10 microohms. The resistance of the specimen continues to decrease with increasing temperature up to 1300°C and the end of the transformation -- A_f -- could not be recorded on the available equipment. On cooling no hysteresis is exhibited; because of the scatter no unambiguous break in the resistance vs. temperature curve such as in Figure 8 can be obtained.

Following the resistance measurements, the ends of the rods were polished and etched at room temperature. Metallographic examination at room temperature revealed

parallel markings (Figures 10 and 12) and chevron-like bands containing parallel markings (Figure 11) indicative of martensitic transformation above room temperature with lattice invariant shear part of the transformation distortion apparently of the twinning type as in AuCd alloys.[8] To study the transformation morphology, hot stage metallographic work on these alloys was undertaken. From Figures 7, 8, and 9 it can be seen that polishing any one of the three alloy specimens in the reference parent phase above M_s would be prohibitively difficult and hence they were polished at room temperature in the product phase. The "inverse" surface upheavals and markings were observed on heating from "martensite" to "austenite."

On heating a specimen of alloy 1 (45.8 at.% Ru) polished at room temperature, parallel markings appeared at about 230°C (Figure 13a), which indicated the start of the reverse reaction from "martensite" to "austenite." The parallel markings became more defined as the specimen was heated to 550°C, but on cooling to room temperature the parallel markings remained. The surface did not appear flat under such conditions since the markings due to the "austenite" to "martensite" reaction were parallel to, but not identical with the first "inverse martensite to austenite" markings. However, on heating to 1600°C and cooling, a second set of markings at an angle to the previously mentioned set appeared at about 490°C (Figure 13b) indicating the "austenite" to "martensite" reaction

had already begun with markings appearing on another (presumably crystallographically equivalent) plane. The second set of markings became more defined as the specimen was cooled to room temperature (Figure 13c), and on cycling between 550°C and 100°C the second set of markings disappeared on heating and reappeared on cooling. The microstructure on heating to 550°C always remained the same and hence it was the reference state, the role which the polished surface of "austenite" would have played if it could have been polished at 550°C.

Alloy 2 (51.1 at.% Ru) showed a rather different behavior. On heating the specimen, which had been polished at room temperature, markings began to appear at about 700°C; the surface at 750°C is shown in Figure 14a. These markings were arranged in chevron like bands, and the markings in the neighboring bands were almost perpendicular to each other. On further heating the broad bands enclosing the finer markings began to tilt relative to each other at about 800°C and alternate bands appeared darker as the temperature was increased as shown in Figure 14b at 830°C and in Figure 14c at 1000°C. On cooling to room temperature from 1000°C, the broad bands tilted back to give almost a flat surface, but the finer markings inside them remained to give a microstructure similar to Figure 14a. However, on heating the specimen to 1600°C and cooling to room temperature a second set of alternate dark and bright bands at an angle to the previously mentioned one appeared (Figure 14d), and the surface was too rumpled

to observe any fine markings inside the second set of bands. This indicates that when the specimen was heated to just above A_f the bands always formed on the same crystallographic plane as the previous time it was cooled giving a nearly flat surface, but when the specimen was heated to 1600°C, which is well above A_f, the transformation took place on another presumably crystallographically equivalent plane and hence the bands appeared at an angle to the first set of "inverse martensite to austenite" bands. On cycling between 1000°C and 700°C the second set of bands disappeared on heating and reappeared on cooling, while the first set always remained serving as the reference state.

In alloy 3 (55.8 at.% Ru) parallel markings appeared at 900°C on the surface, which had been polished at room temperature, and when the specimen was further heated to 1600°C and cooled to 800°C parallel markings at an angle to the original ones appeared (Figure 15a). On cycling between 1300°C and 800°C the markings, which appeared on cooling from 1600°C to 800°C, disappeared on heating (Figure 15b) and reappeared on cooling in the same direction though not at the same place (Figure 15c). The marked surface, which appeared on heating the polished surface for the first time, could always be seen on subsequent heatings and hence was the reference state. A_f for this alloy was estimated to be around 1300°C. (Note that this could not be obtained from resistance measurements.)

The crystal structures of the low temperature phases of all the alloys were determined at room temperature by

the powder method. However it had to be ascertained whether there was any effect of particle size on the transformation. Magnetic susceptibility of both bulk and powder specimens was measured; alloy 2 (51.1 at.% Ru) was chosen for the magnetic study because its transformation range was most convenient for the equipment employed. The force on the alloy (which is directly proportional to the magnetic susceptibility) is shown as a function of temperature for bulk and powder specimens in Figures 16 and 17 respectively. The high temperature phase is paramagnetic and its magnetic susceptibility shows no temperature dependence; the low temperature phase is also paramagnetic, but its magnetic susceptibility increases with increasing temperature. Note that the curves show the transformation occurring over the same temperature region as indicated by resistance measurements, c.f. Figure 8, and the powders transform like bulk specimens except for what could be interpreted as hysteresis in that part of the transformation occurring between 700°C and 800°C, although this may be experimental scatter in the temperature measurements due to the way the thermocouple was placed. A change in the slope of the curve during transformation is shown in Figure 16 and it occurs essentially at the same temperature as the break in resistance vs. temperature curve of Figure 8; the break in the powder curve of Figure 17 is not clearly defined.

The room temperature structures of the alloys were determined from their powder patterns, which were indexed by matching the observed 'd' values with the 'd' values

calculated from approximate lattice parameters. Cohen's method[9] programmed for an IBM 7094 computer was used to calculate the lattice parameters. The results are shown in Table 3.

Table 3. Crystal Structure and Lattice Parameters of Alloys 1, 2, and 3 at Room Temperature

Alloy #	Crystal Structure	Lattice Parameters Å	c/a	c/b
1	face-* centered tetragonal	a = 4.388 ± .005 c = 3.311 ± .005	.755	-
2	face-centered orthorhombic	a = 4.373 ± .005 b = 4.228 ± .005 c = 3.401 ± .005	.788	.804
3	face-centered orthorhombic	a = 4.295 ± .005 b = 4.192 ± .005 c = 3.439 ± .005	.801	.820

A few super structure lines could be observed in each of the powder patterns and the alloys are probably ordered.

As mentioned in the introduction, Raub and Fritzsche[4] reported the low temperature phase to be body-centered tetragonal in alloys having compositions between 41 and 46.5 at.% Ru and face-centered orthorhombic for alloys having compositions between 47 and 58 at.% Ru. However to understand the relationship among the product phases as well as how they are related to the parent phases, it is much more instructive in the first mentioned composition range to choose in place of the body-centered tetragonal cell a face-centered tetragonal cell, which can be

*The reasons for choosing this unit cell rather than the smaller equivalent body-centered tetragonal unit cell are described in the text.

formed by delineating such a cell within four body-centered tetragonal cells as in Figure 18b, with a_f the a parameter of the face-centered tetragonal cell, equal to $\sqrt{2}$ times a_b, the a parameter of the body-centered tetragonal cell. Thus focussing on an arbitrary unit cell in the parent CsCl type phase (assumed), which is face-centered tetragonal, with c/a of $1/\sqrt{2}$ or .707, and how it is distorted (as can be seen in Figure 18) to either a face-centered tetragonal cell with a different c/a ratio or to a face-centered orthorhombic cell with an anisotropic distortion in the plane perpendicular to the 'c' axis permits a rather simple unified approach to all transformations in the composition range examined.

The behavior of alloy 2 (51.1 at% Ru) can be interpreted as follows. It can be seen in Figures 7 and 8 that the slope of the curve for alloy 1 (45.8 at.% Ru) is essentially constant and is almost the same as the slope of the curve for alloy 2 between 800°C and 900°C. Since the low temperature phase of alloy 1 can be described as a face-centered tetragonal phase, it is suggested that in case of alloy 2 the high temperature CsCl type phase (assumed) transforms to a face-centered tetragonal phase on cooling and this face-centered tetragonal phase transforms to a face-centered orthorhombic phase with small distortions on further cooling. The start of the f.c.t. to f.c.o. transformation occurs before completion of the CsCl to f.c.t. transformation; this accounts for the change in the slope of the resistance vs. temperature curve during transformation (Figure 8). It is also to be noted that on cooling the f.c.t. to f.c.o. transformation

cannot finish before the CsCl to f.c.t. transformation does. This model can also account for the hot-stage micrographic results of alloy 2. The appearance of fine parallel markings (Figure 14a) arranged in chevron like bands on the surface polished at room temperature and heated to 750°C is consistent with a reverse reaction f.c.o. to f.c.t., while tilting of the broad bands above 800°C (Figure 14b) fits with the f.c.t. to CsCl reaction.

In case of alloy 1, the cubic to f.c.t. transformation is complete well above the room temperature; there may indeed be a f.c.t. to f.c.o. transformation below room temperature. In case of alloy 3 (55.8 at.% Ru) because of the temperature limitations of the resistivity apparatus employed, experimental difficulties in hot-stage microscope, and the absence of high temperature vacuum X-ray camera, it cannot be definitely stated at this time whether a cubic to f.c.t. transformation precedes the transformation in Figure 9, which would then be interpreted as f.c.t. to f.c.o. on cooling, or whether this curve shows a direct transformation from the high temperature cubic phase to the f.c.o. phase, which is observed at room temperature. In any event, to show the reasonableness of this approach, the data of Raub and Fritzsche[4] are plotted together with the results of this investigation in Figure 19 after "converting" their b.c.t. cells to f.c.t. cells by multiplying their $\underline{a}$ values by $\sqrt{2}$. It can be seen from this figure that the f.c.o. cell differs very little from the

f.c.t. cell and hence can also be derived from the cubic phase, although probably by a two step process with an intermediate f.c.t. phase. Furthermore, even at room temperature c/a and c/b ratios of product phases are not very different from $\sqrt{2}/2 = .707$ consistent with the model proposed above; c/a and c/b ratios may be very close to .707 at the transformation temperatures.

IV. CONCLUSIONS

It can be concluded (and/or inferred) that near-equiatomic Nb-Ru alloys transform martensitically on cooling and the transformation temperatures decrease markedly with increasing Nb content. In case of alloys near the exact stochiometry (eg. 51.1 at.% Ru) the transformation appears to occur in two steps; i.e., CsCl to f.c.t. and f.c.t. to f.c.o., on cooling. In alloys of lower Ru content (eg. 45.8 at.% Ru) only one step of what may be a two step transformation process occurs above room temperature. On cooling below room temperature a f.c.t. to f.c.o. transformation may occur following the CsCl to f.c.t. transformation reported here. In alloys of higher Ru content (eg. 55.8 at.% Ru) it cannot be concluded definitely whether the transformation, which is observed between 950°C and 1300°C, consists of two steps or one step; there may be a CsCl to f.c.t. transformation occurring at a temperature higher than 1300°C. The transformations are reversible with hysteresis widths less than 10°C and hence the transformation strains are probably quite small. The banded microstructure of the product phases constitute good evidence that the lattice invariant shear is twinning, as in InTl,[10] some iron base alloys,[11] and the prototype CsCl to almost f.c.o. transformation in AuCd,[8] which stimulated the WLR crystallographic theory of martensitic transformation.[8,12] In the case of alloys under consideration, particle size has little effect on the martensitic reaction. Further work is indicated to determine the structure of all phases and to examine the details of the transformation.

Figure 1. Niobium-ruthenium phase diagram.[5]

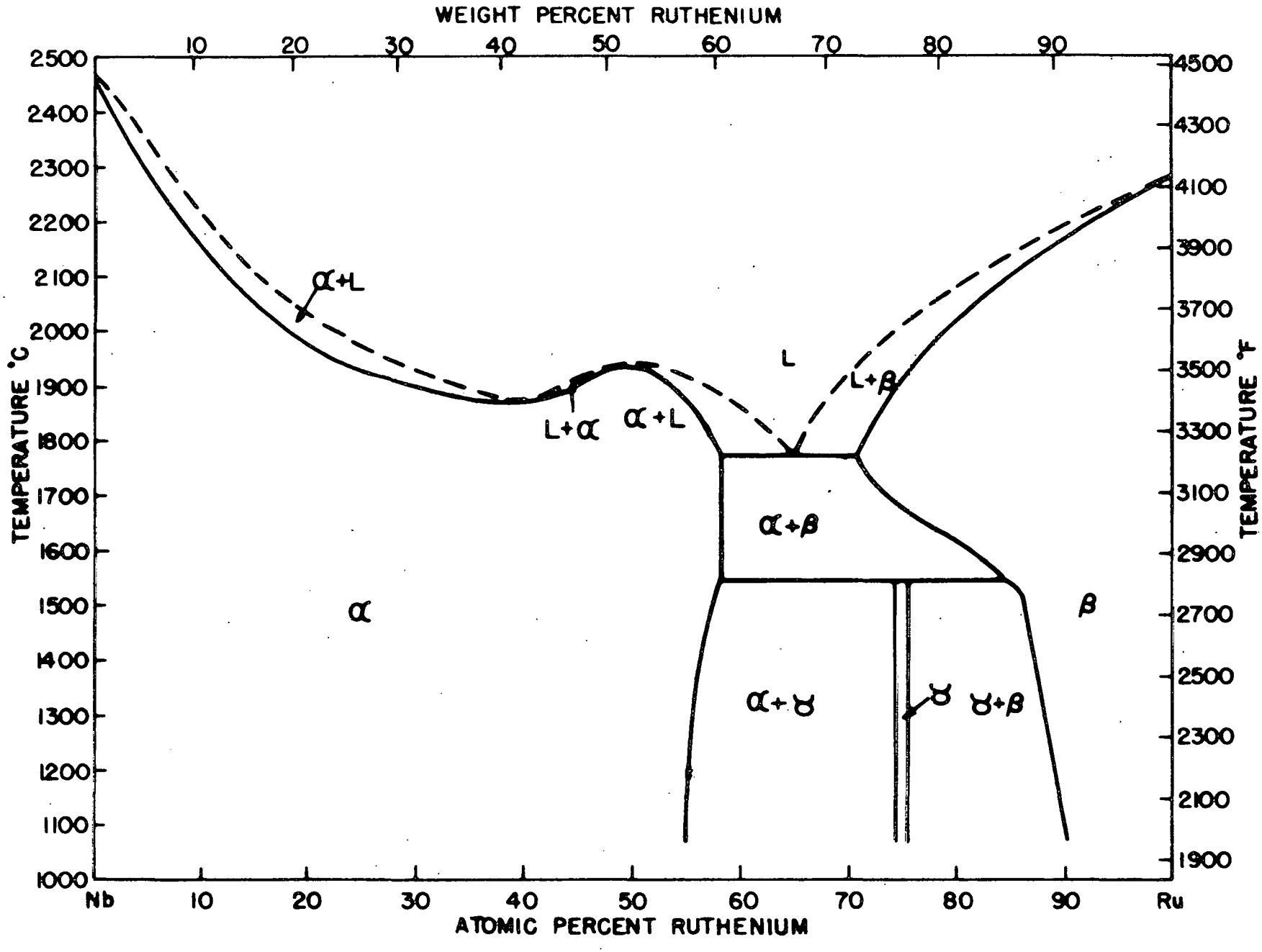
WEIGHT PERCENT RUTHENIUM
10 20 30 40 50 60 70 80 90
2500 2400 2300 2200 2100 2000 1900 1800 1700 1600 1500 1400 1300 1200 1100 1000
TEMPERATURE °C
4500 4300 4100 3900 3700 3500 3300 3100 2900 2700 2500 2300 2100 1900
TEMPERATURE °F
α+L
L
L+β
L+α
α+L
α+β
α
β
α+γ
γ
γ+β
Nb 10 20 30 40 50 60 70 80 90 Ru
ATOMIC PERCENT RUTHENIUM

Figure 2. Die used for preparing powder compacts.

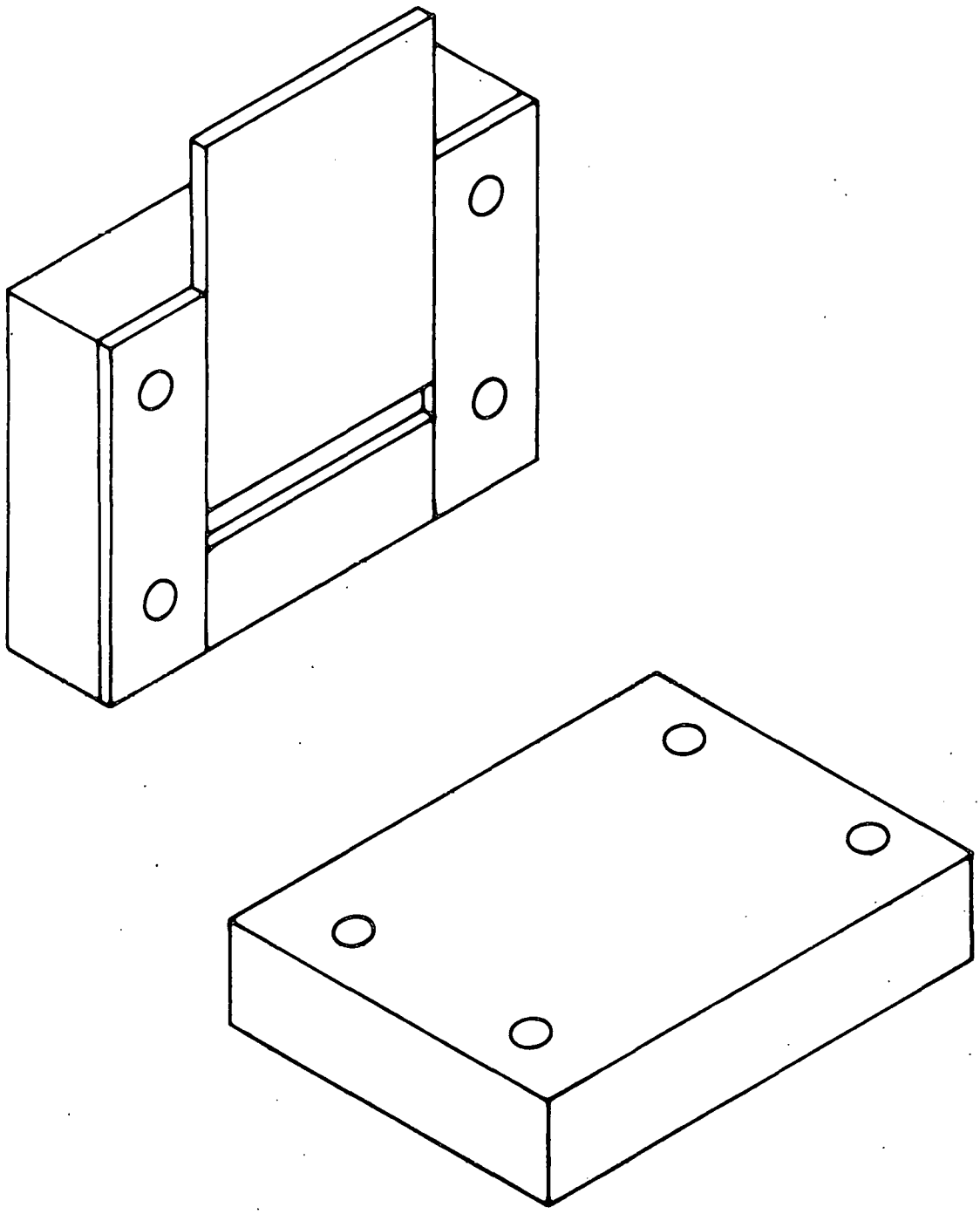

Figure 3. Schematic circuit diagram of apparatus used for measurement of electrical resistance of the specimens.

1. 1 ohm standard resistor
2. Standard cell
3. Reversible AC motor
4. 1 ohm variable resistor
5. Specimen

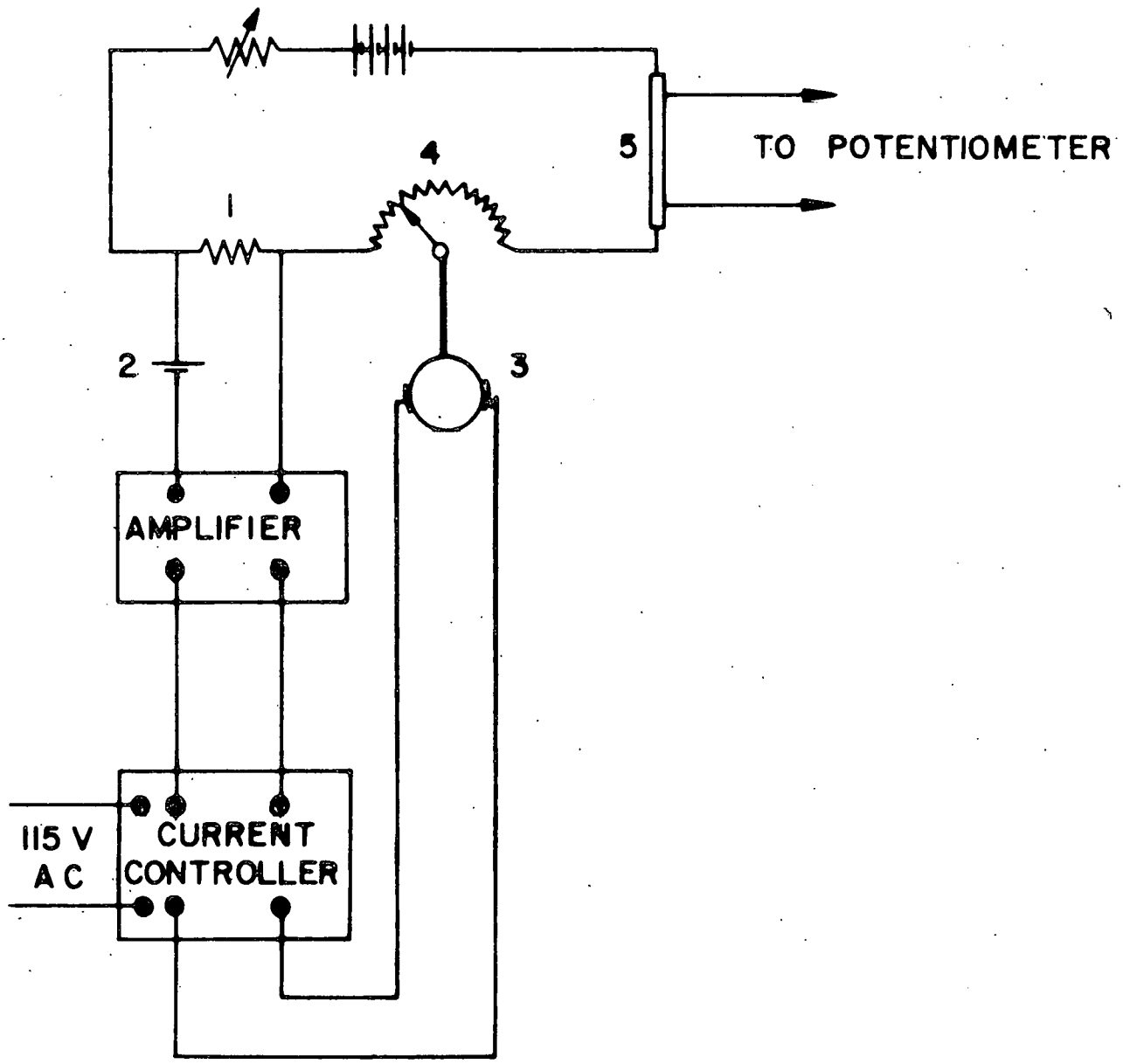
TO POTENTIOMETER
5
4
1
2
3
AMPLIFIER
115 V
A C
CURRENT
CONTROLLER

Figure 4. Induction heating of the specimen.

1. Induction coil
2. Outer alumina tube
3. Inner alumina tube
4. Tantalum susceptor
5. Alumina disc reflectors
6. Specimen
7. Current leads
8. Potential leads
9. Thermocouple

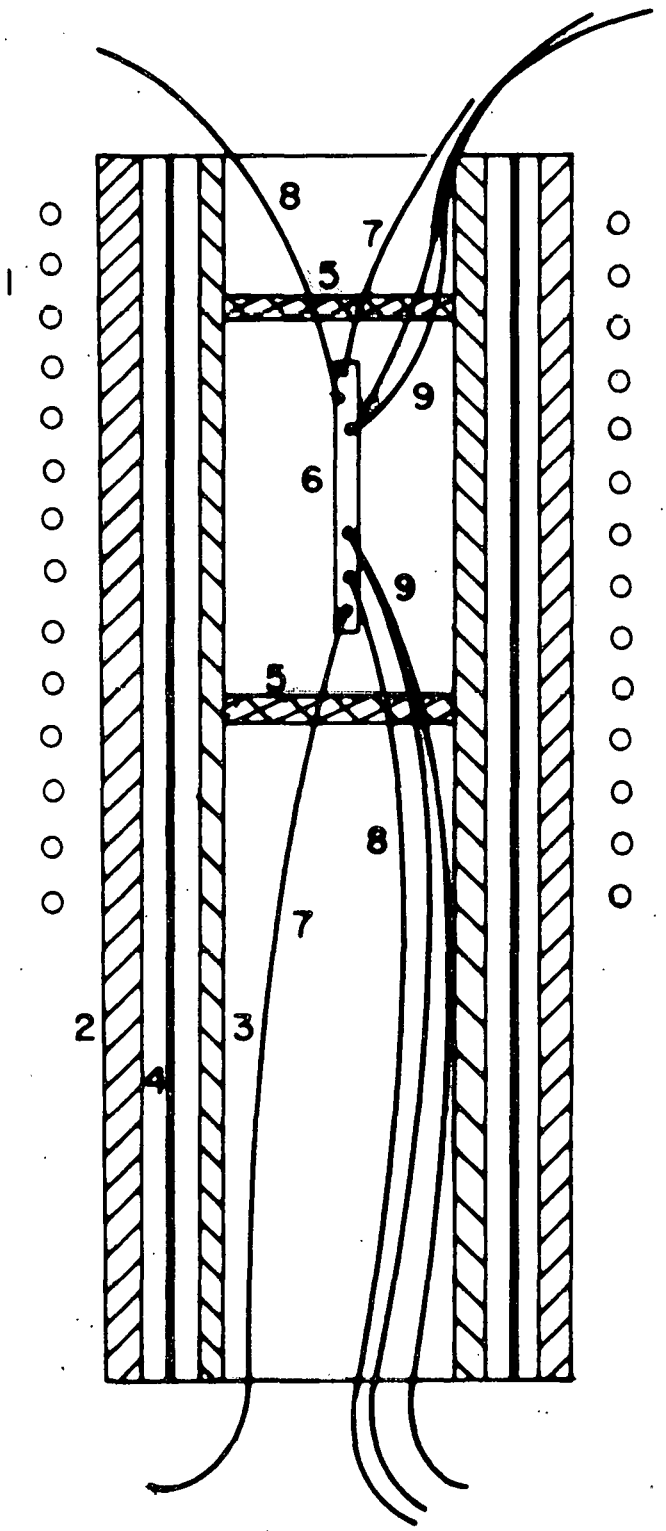
1
2
3
4
5
6
7
8
9
8
7
3
9
6
9
5
8
7
2
3
4

Figure 5. Change in electrical resistivity of Ta (99.95 wt.% pure) with temperature.

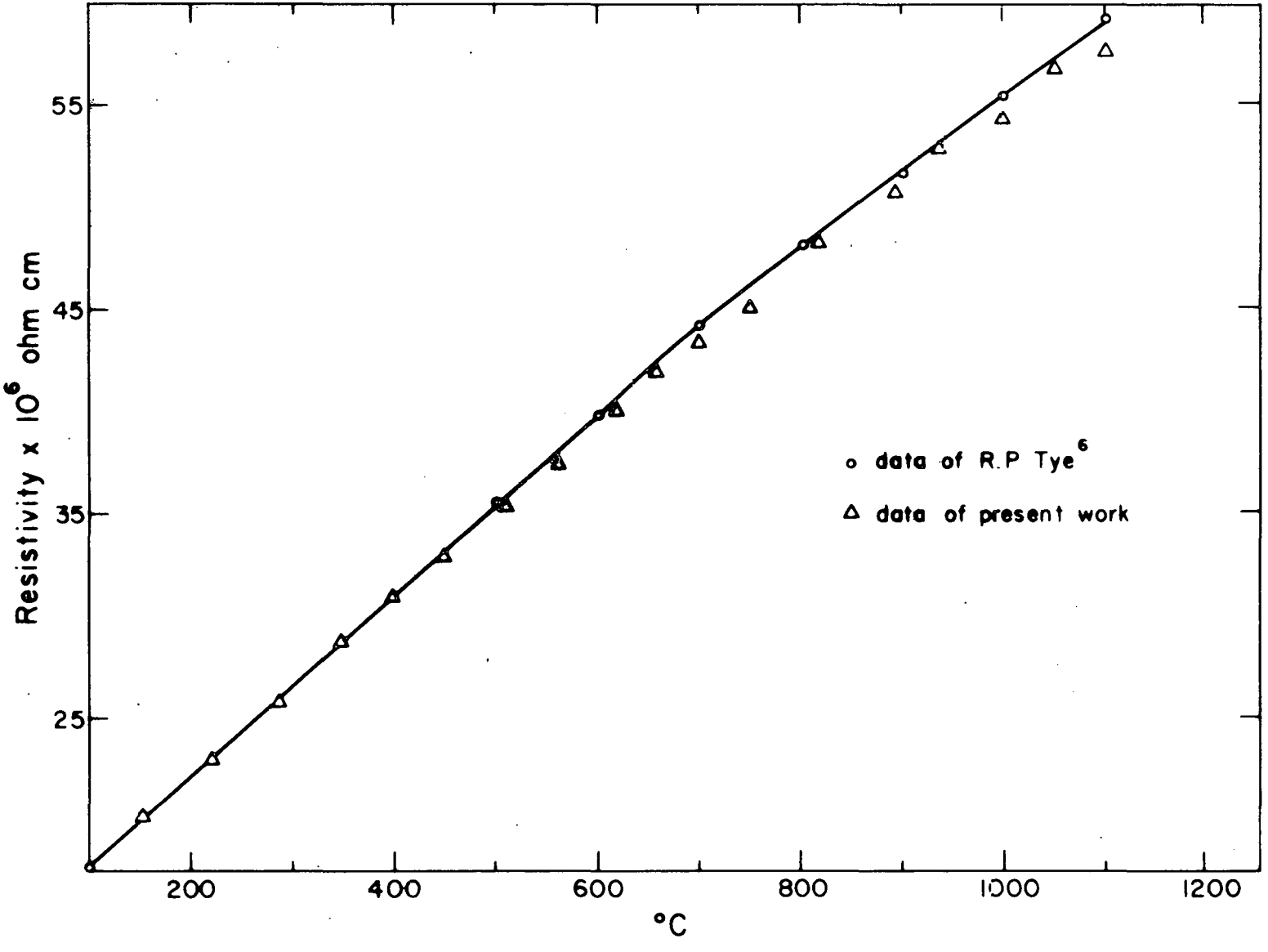
Resistivity x 10^6 ohm cm
55
45
35
25
200
400
600
800
1000
1200
°C
o data of R.P Tye[6]
Δ data of present work

Figure 6. Heating element used in hot stage.

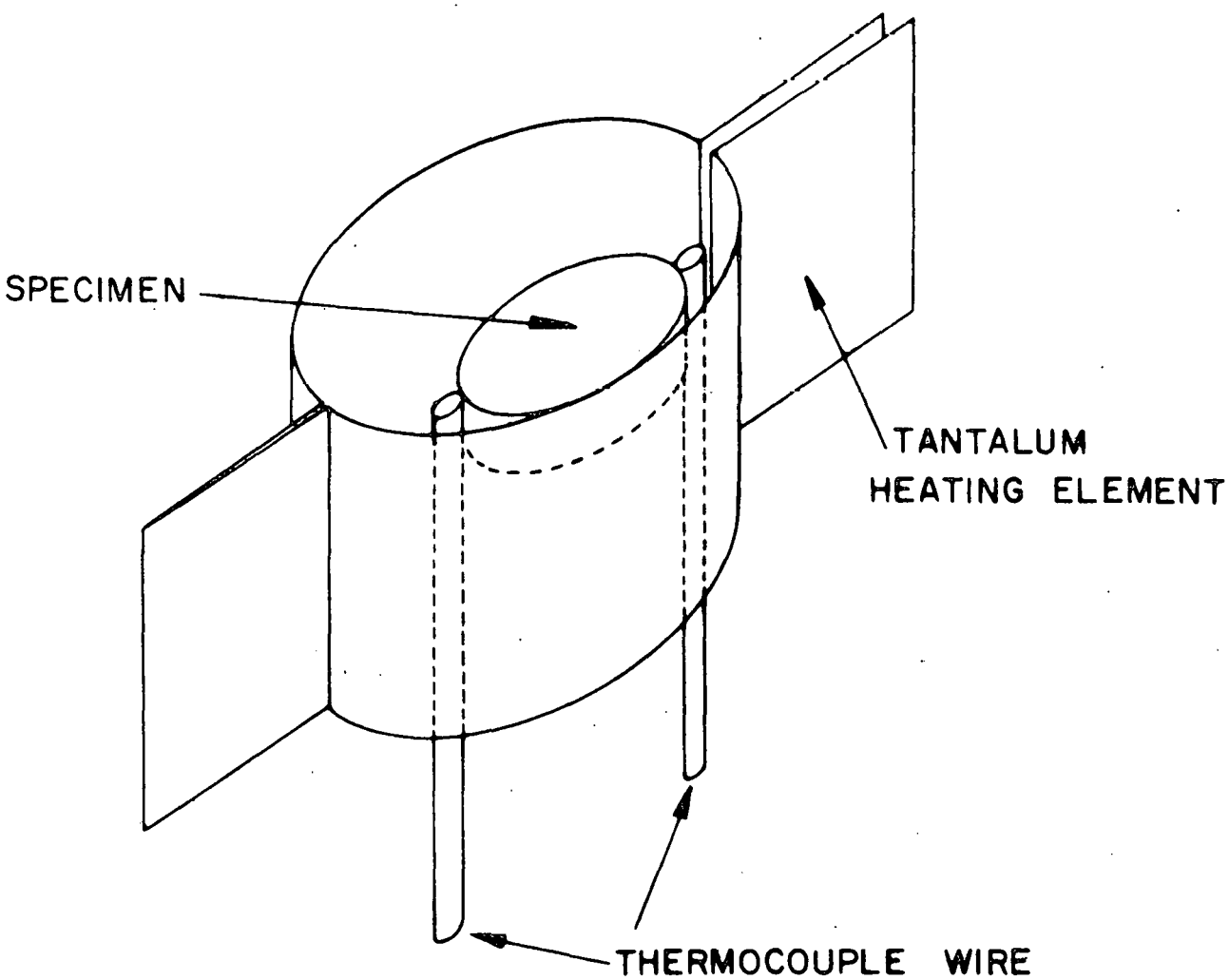
SPECIMEN
TANTALUM
HEATING ELEMENT
THERMOCOUPLE WIRE

Figure 7. Electrical resistance of alloy 1 (45.8 at.% Ru) vs. temperature.

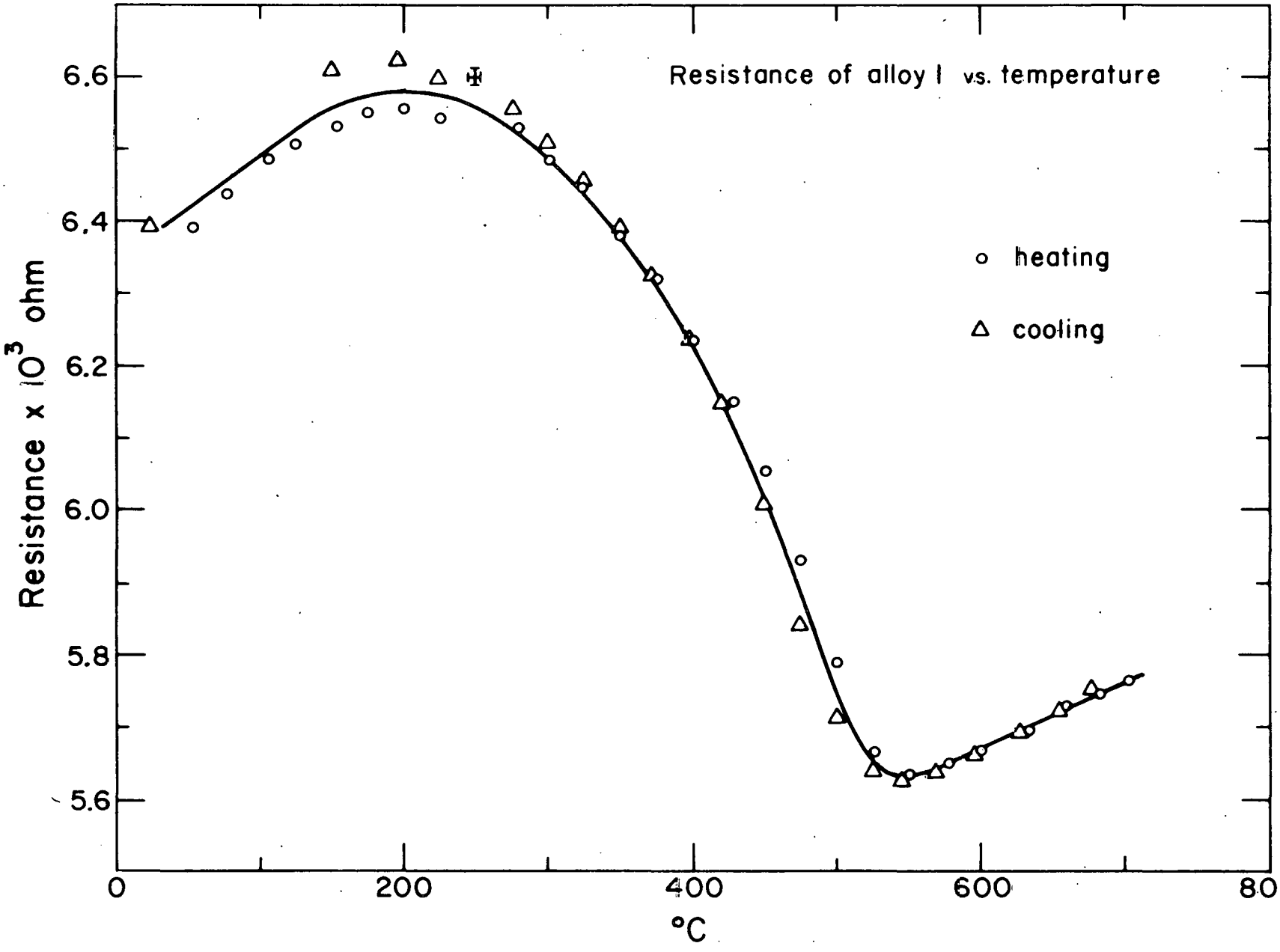
Resistance of alloy I vs. temperature
o heating
Δ cooling
Resistance x 10^3 ohm
6.6
6.4
6.2
6.0
5.8
5.6
0
200
400
600
800
°C

Figure 8. Electrical resistance of alloy 2 (51.1 at.% Ru) vs. temperature. Note the change in the slope of the curve during transformation at about 790°C.

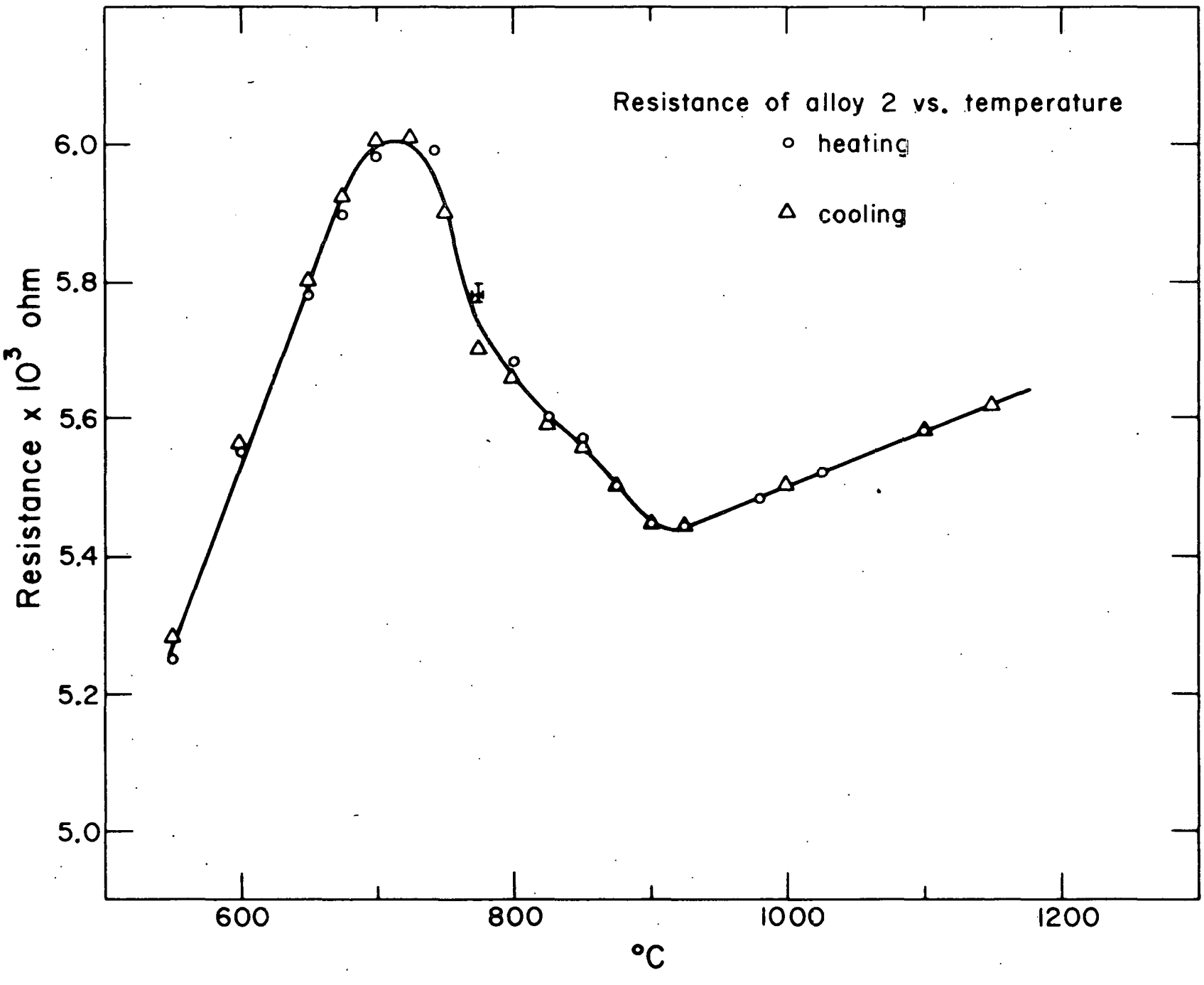
Resistance of alloy 2 vs. temperature
heating
cooling
Resistance x 10^3 ohm
6.0
5.8
5.6
5.4
5.2
5.0
600
800
1000
1200
°C

Figure 9. Electrical resistance of alloy 3 (55.8 at.% Ru) vs. temperature. The vertical and horizontal bars show the estimated errors in measurement of resistance and temperature respectively.

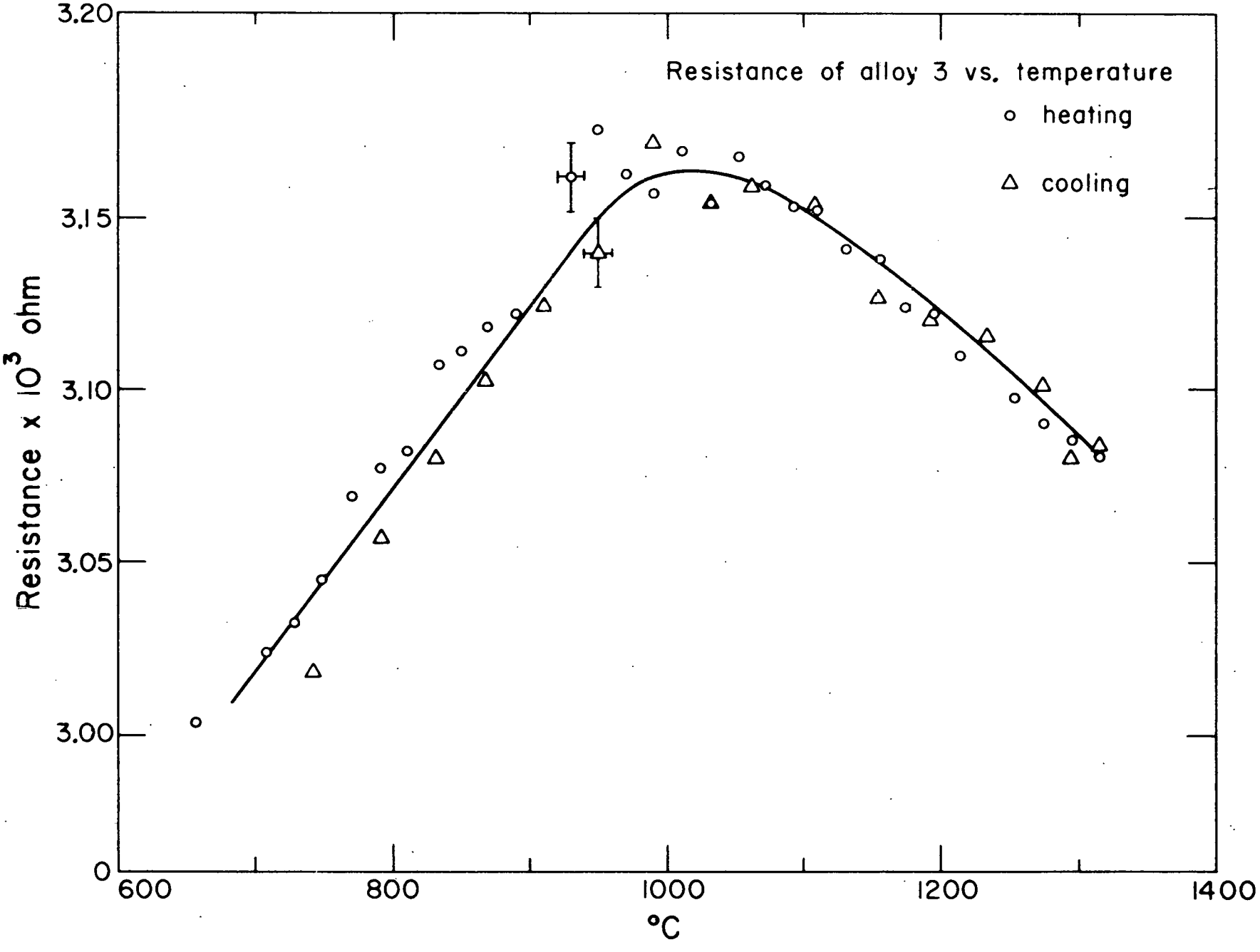
Resistance of alloy 3 vs. temperature
heating
cooling
Resistance x 10^3 ohm
3.20
3.15
3.10
3.05
3.00
0
600
800
1000
1200
1400
°C

Figure 10. Room temperature micrograph of alloy 1 (45.8 at.% Ru) polished and etched at room temperature following growth and one cycle of transformation. Note the parallel markings. X150

Figure 11. Room temperature micrograph of alloy 2 (51.1 at.% Ru) polished and etched at room temperature following growth and one cycle of transformation. Note the broad bands containing parallel markings. The markings in alternate bands, which appear bright, can be seen, though they could not be etched properly. X400

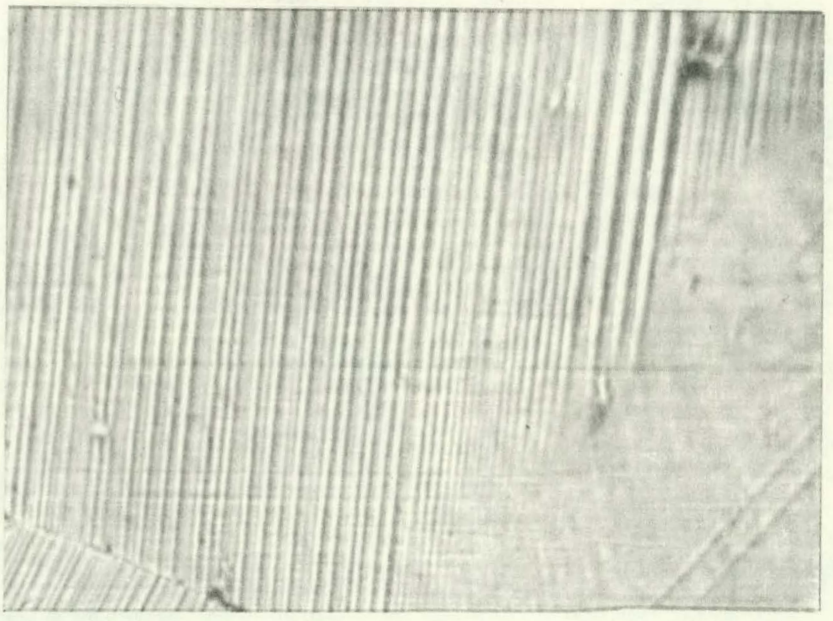

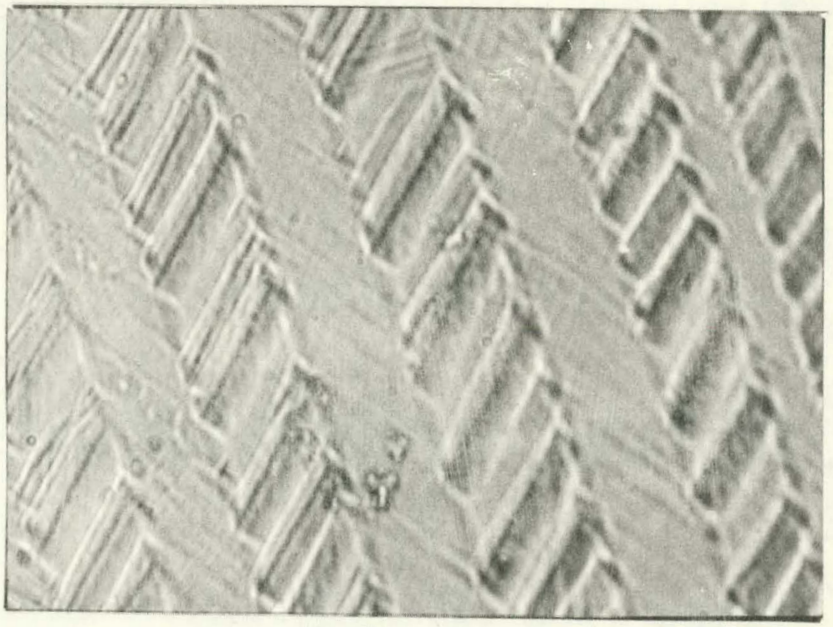

Figure 12. Room temperature micrograph of alloy 3 (55.8 at.% Ru) polished and etched at room temperature after growth and one cycle of transformation. X256

Figure 13a. Photograph of the surface of alloy 1 (45.8 at.% Ru) polished at room temperature and heated to 230°C. Parallel markings have appeared on the polished surface. X500

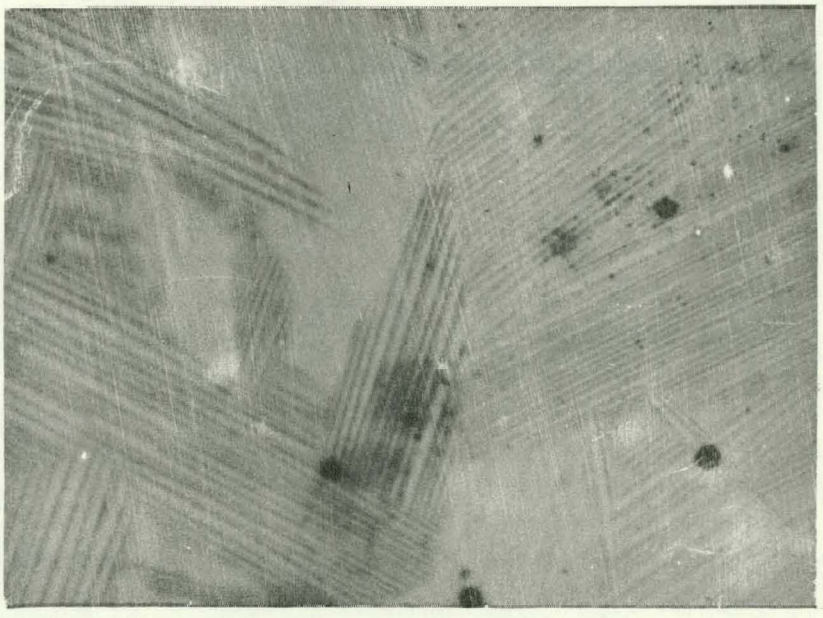

Figure 13b. Appearance of the surface of alloy 1 after it was heated from conditions of Figure 13a to 500°C, cooled to room temperature and again heated to 1600°C and cooled to 490°C. Note the appearance of a new set of markings at an angle to the set seen in Figure 13a. X500

Figure 13c. Appearance of the surface of alloy 1 after it was cooled to room temperature from conditions of Figure 13b. X500

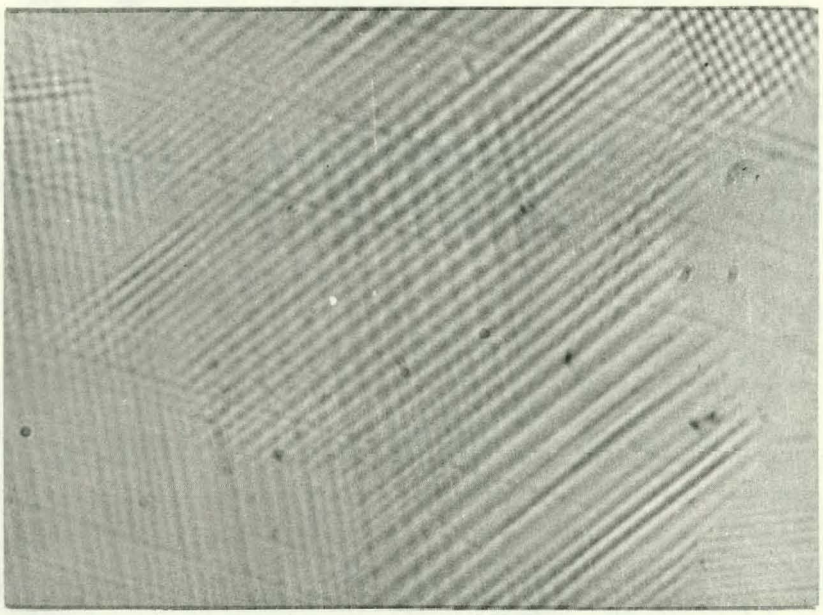

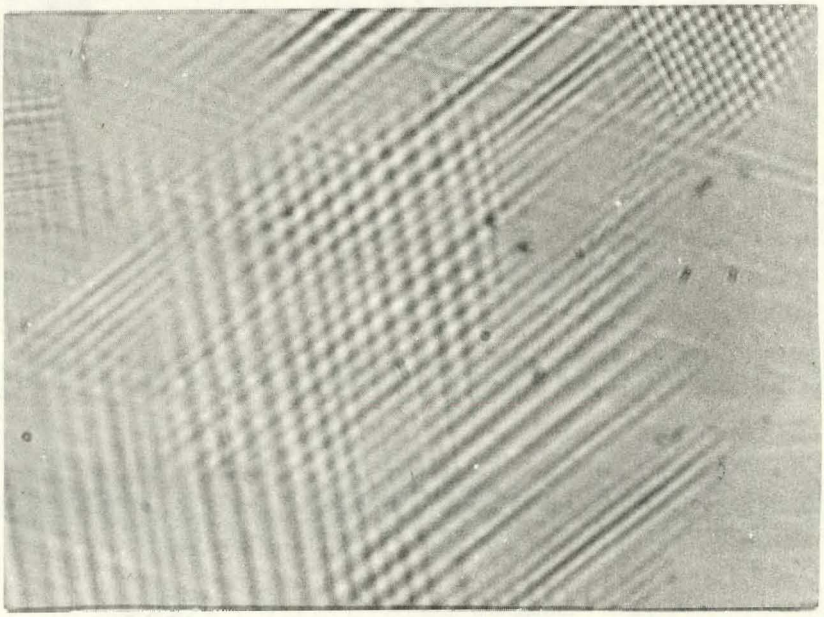

Figure 14a. Micrograph of the surface of alloy 2 (51.1 at.% Ru) polished at room temperature and heated to 750°C. Note the appearance of chevron like bands each enclosing inside it a set of parallel markings, which are nearly perpendicular to the markings in the neighboring band. X100

Figure 14b. Photograph of the surface of alloy 2 heated from conditions of Figure 14a to 830°C. The broad bands have begun to tilt and hence alternate bands appear dark. X100

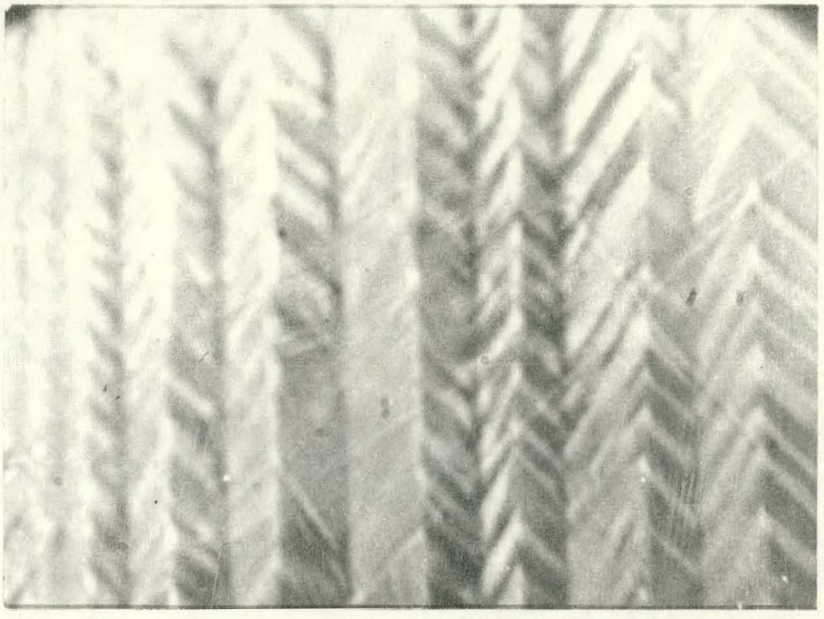

Figure 14c. Appearance of the surface of alloy 2 when it was further heated to 1000°C. The alternate bands appear darker than in Figure 14b. X100

Figure 14d. Photograph of alloy 2 taken at room temperature after it was cooled from conditions of Figure 14c to room temperature and subsequently heated to 1600°C and cooled to room temperature. Note that a second set of alternate dark and bright bands have appeared at an angle to the original bands of Figure 14c. X100

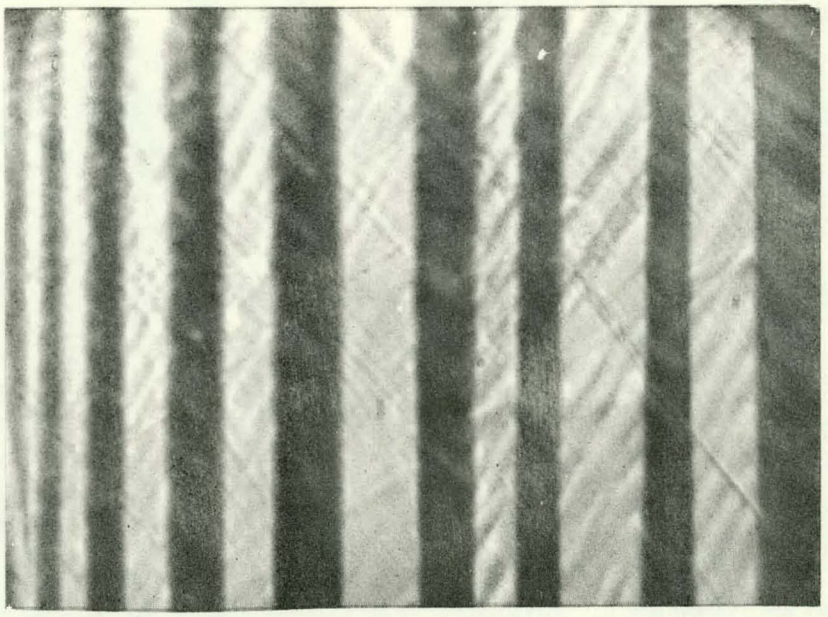

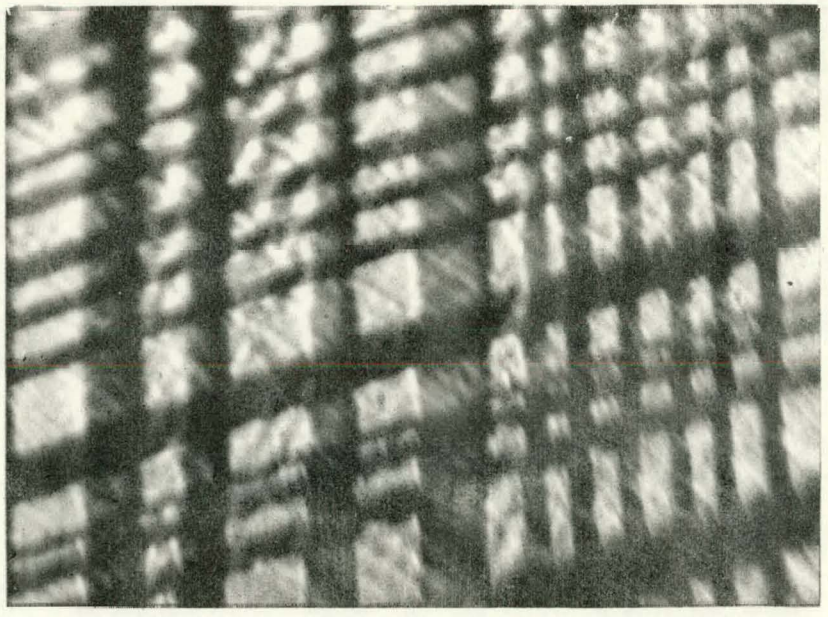

Figure 15a. Condition of the surface of alloy 3 (55.8 at.% Ru) polished and etched at room temperature, heated to 1600°C, and cooled to 800°C. Note the criss-crossing sets of parallel markings. X400

Figure 15b. Photograph of the surface of alloy 3 after it was heated from conditions of Figure 15a to 1300°C. Note that in contrast to Figure 15a, there are no crossed markings and that markings of one variant have disappeared on heating leaving the "reference state." X400

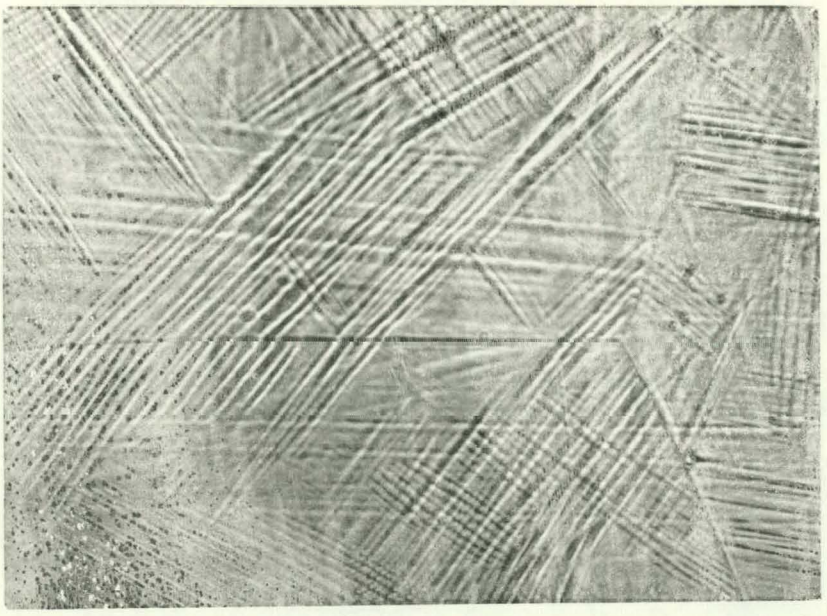

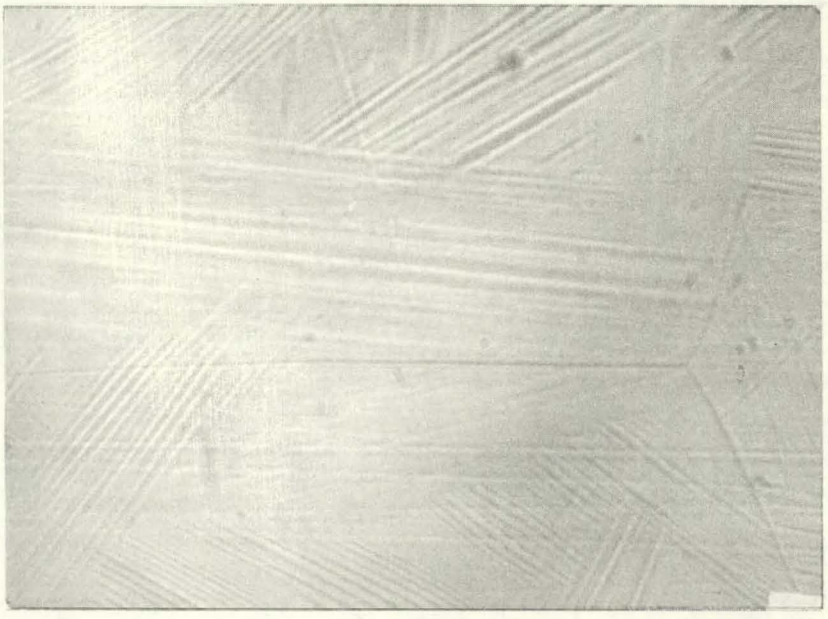

Figure 15c. Micrograph of the surface of alloy 3 cooled from conditions of Figure 15b to 800°C. New markings crossing the markings Figure 15b have appeared in the same direction as the markings, which disappeared on heating from conditions of Figure 15a to 1300°C. X400

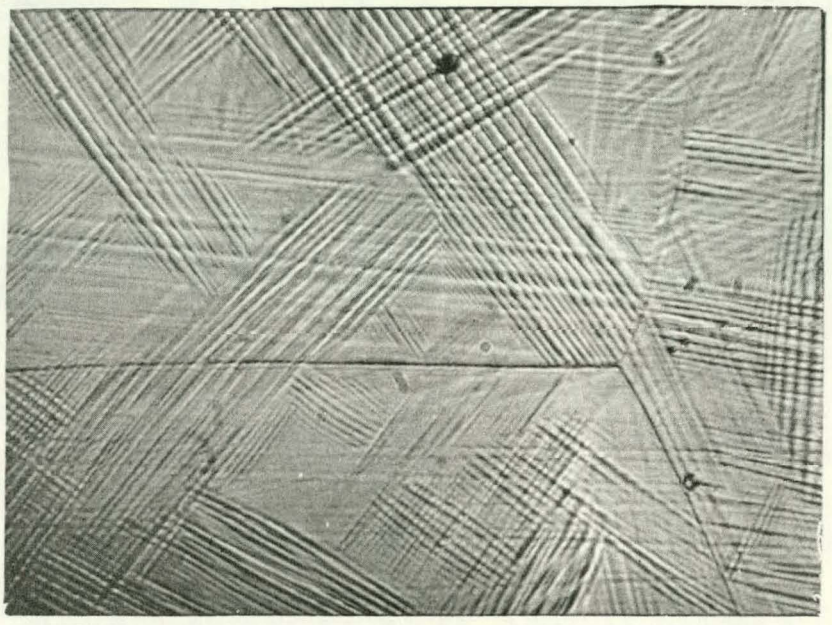

Figure 16. Change in magnetic susceptibility of bulk specimens of alloy 2 (51.1 at.% Ru) with temperature. Comparing with Figure 8 it can be seen that the changes in slope of both the curves occur at the same temperatures.

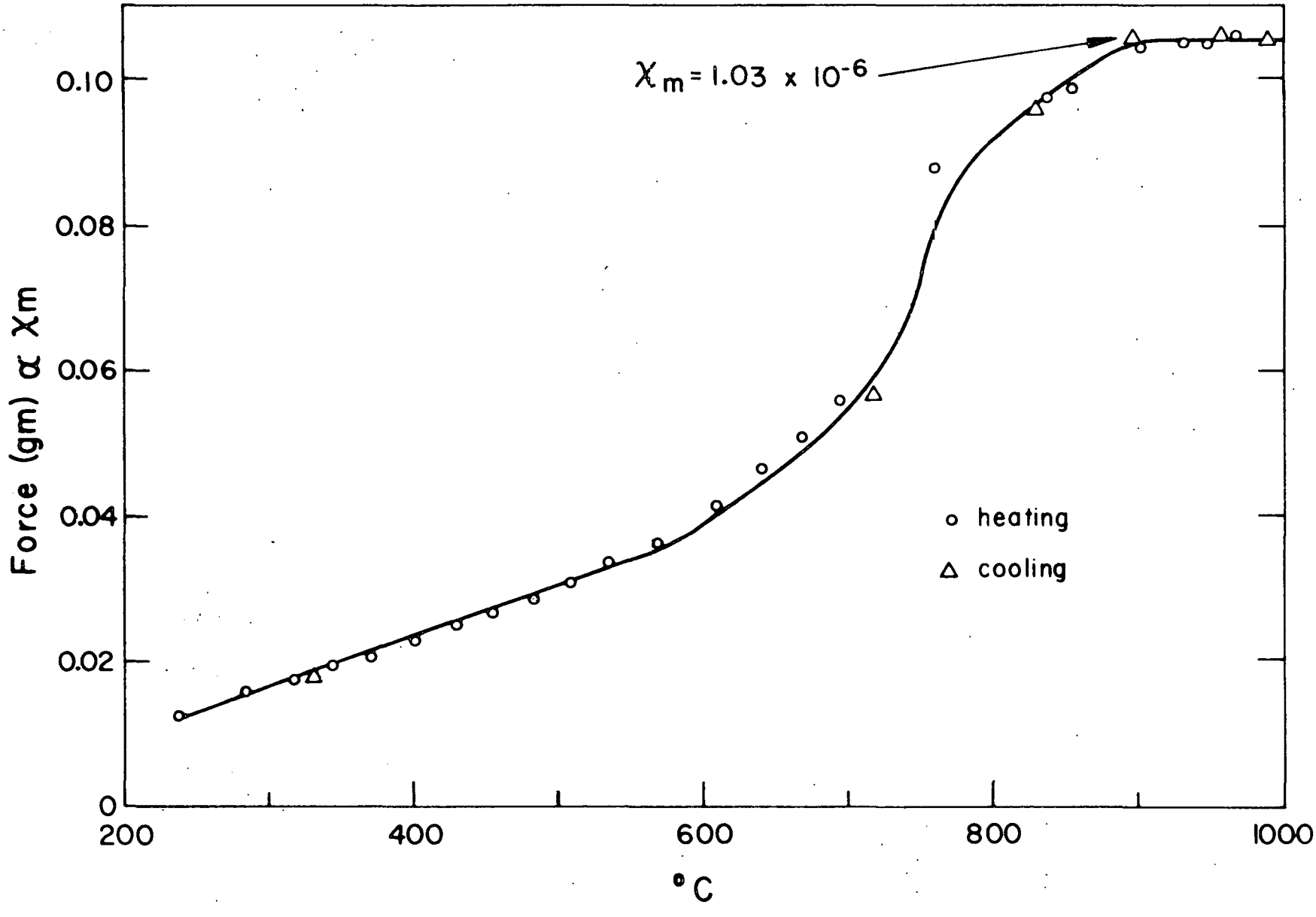
$\chi_m = 1.03 \times 10^{-6}$
Force (gm) α χm
0.10
0.08
0.06
0.04
0.02
0
200
400
600
800
1000
°C
o heating
Δ cooling

Figure 17. Change in magnetic susceptibility of powders of alloy 2 with temperature.

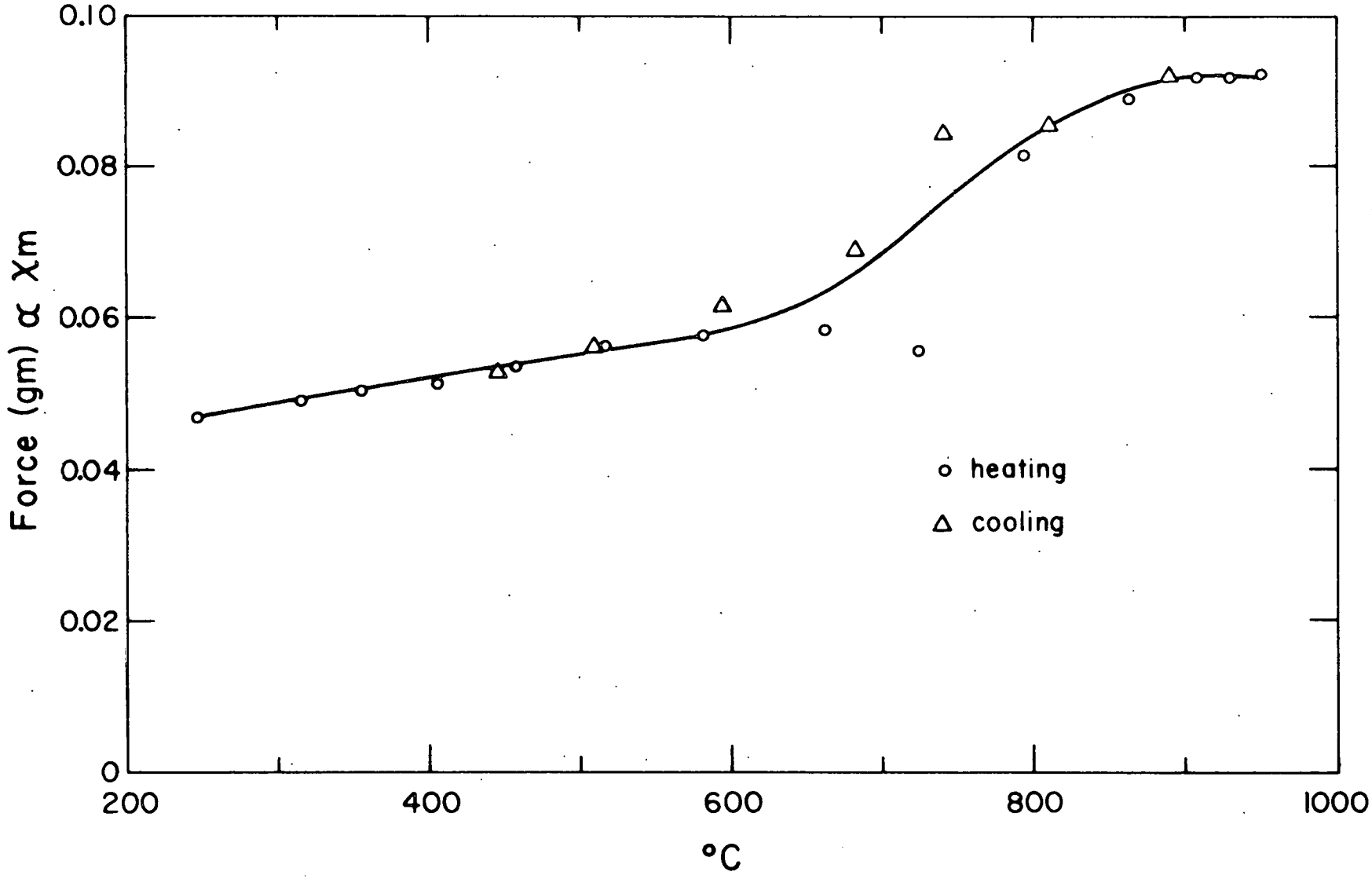
0.10
0.08
0.06
0.04
0.02
0
Force (gm) α χm
200
400
600
800
1000
°C
heating
cooling

Figure 18. (a) Untransformed CsCl structure in which a f.c.t. cell is delineated. $a = \sqrt{2}a_o$, $c/a = 1/\sqrt{2} = .707$.

(b) Face-centered tetragonal cell obtained due to transformation distortion, so that c/a is somewhat greater than $1/\sqrt{2}$. This lattice can also be described equivalently by a body-centered tetragonal cell, a distorted CsCl structure with c/a slightly greater than 1.

(c) Face-centered orthorhombic cell produced due to a distortion, which is anisotropic in the plane perpendicular to the 'c' axis. Note how (c) can be obtained from (b) by a slight anisotropic distortion.

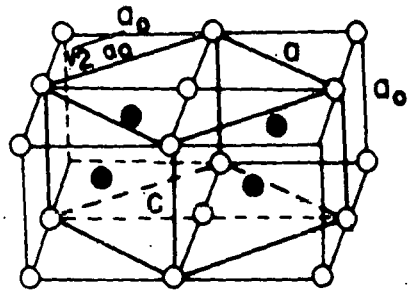

A. CsCl

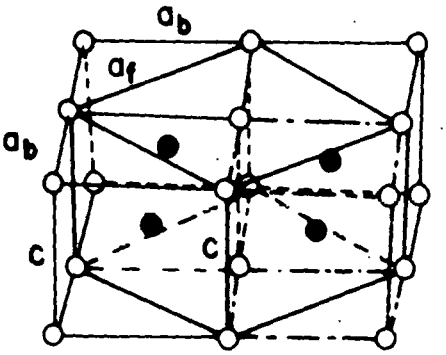

B. FACE-CENTERED TETRAGONAL

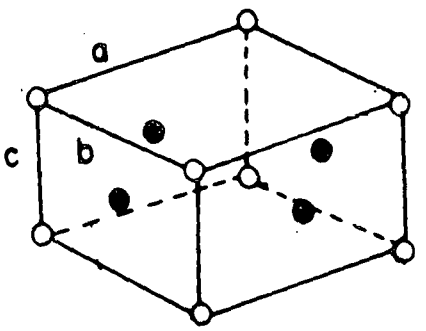

C FACE-CENTERED ORTHORHOMBIC

Figure 19. Variation of room temperature lattice parameters of near-equiatomic Nb-Ru alloys with composition. The a parameters of the tetragonal phase obtained by Raub and Fritzsche[4] have been multiplied by $\sqrt{2}$.

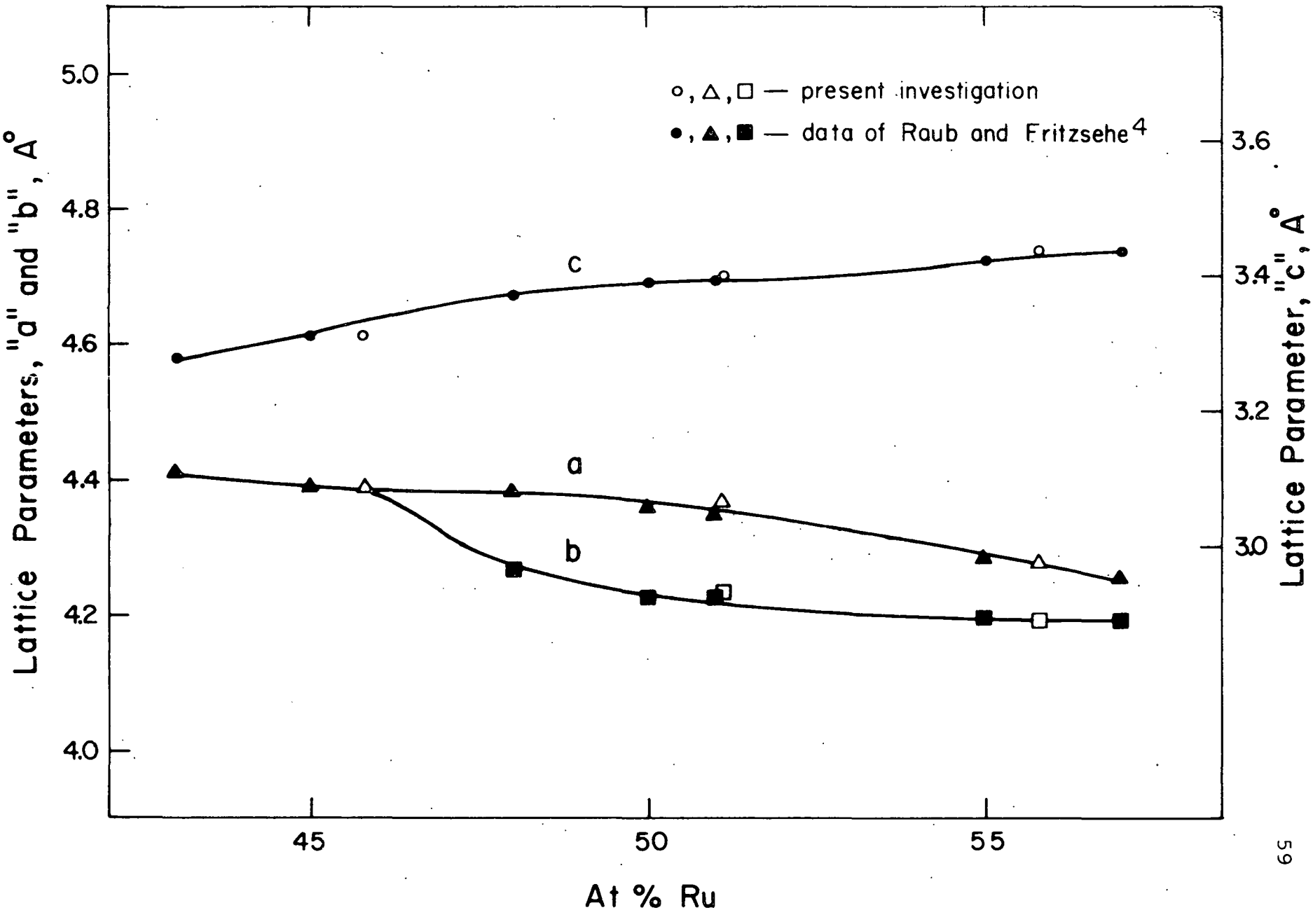
5.0
4.8
4.6
4.4
4.2
4.0
Lattice Parameters, "a" and "b", A°
3.6
3.4
3.2
3.0
Lattice Parameter, "c", A°
45
50
55
At % Ru
o, Δ, □ — present investigation
●, ▲, ■ — data of Raub and Fritzsehe[4]
c
a
b

V. REFERENCES

1. Christian, J. W., Read, T. A., and Wayman, C. M., Intermetallic Compounds. John Wiley and Sons, Inc., New York (1967) 428.
2. Greenfield, P. and Beck, P. A., Trans. A.I.M.E. 206 (1956) 265.
3. Dwight, A. E., Trans. A.I.M.E. 215 (1959) 283.
4. Raub, E. and Fritzsche, W., Z. f. Metallkunde 54 (1963) 317.
5. Kaufmann, Rapperport, and others, Refractory Metal Constitution Diagram, WADD Tech. Report 60-132 (October 1960).
6. Tye, R. P., J. of Less Com. Metals 3 (1961) 13.
7. Gardner, J. A., 1966, Ph. D. Thesis, University of Illinois.
8. Lieberman, D. S., Wechsler, M. S., and Read, T. A., J. of Appl. Phys. 26 (1955) 473.
9. Cohen, M. U., Rev. Sci. Instr. 6 (1935) 68.
10. Burkart, M. W. and Read, T. A., Trans. A.I.M.E. 197 (1953) 1516.
11. Wayman, C. M., Introduction to the Crystallography of Martensitic Transformation. The Macmillan Company, New York (1964)
12. Wechsler, M. S., Lieberman, D. S., and Read, T. A., Trans. A.I.M.E. 197 (1953) 1503.

VI. APPENDIX

X-RAY POWDER PATTERNS

1. Alloy 1
2. Alloy 2
3. Alloy 3

1. Alloy 1 (45.8 at.% Ru)

Radiation	Cu Kα
Crystal Structure Determined	Face-centered tetragonal
Lattice Parameters	a = 4.388 Å
	c = 3.311 Å

hkl	intensity	'd' spacings, Å observed	calculated
111	very strong	2.256	2.264
200	strong	2.194	2.194
002	weak	1.654	1.655
220	medium strong	1.551	1.551
202	medium strong	1.317	1.321
331	strong	1.281	1.280
222	strong	1.130	1.132
400	weak	1.090	1.097
113	weak	1.039	1.040
420	strong	0.982	0.981
402	medium strong	0.912	0.914
313	medium strong	0.862	0.863
422	medium strong	0.845	0.844
511	medium strong	0.834	0.833

2. Alloy 2 (51.1 at.% Ru)

Radiation	Cu Kα
Crystal Structure Determined	Face-centered orthorhombic
Lattice Parameters	a = 4.373 Å
	b = 4.228 Å
	c = 3.401 Å

hkl	intensity	'd' spacings, Å observed	calculated
111	very strong	2.252	2.266
200	strong	2.172	2.186
020	strong	2.110	2.114
002	strong	1.689	1.700
220	strong	1.495	1.521
202	medium strong	1.337	1.342
022	medium strong	1.321	1.325
311	strong	1.273	1.277
131	strong	1.246	1.247
222	strong	1.130	1.133
400	strong	1.091	1.093
113	strong	1.060	1.062
420	strong	0.970	0.971
402	strong	0.918	0.919
313	medium strong	0.874	0.875
133	weak	0.865	0.866
422	medium strong	0.842	0.843
242	medium strong	0.830	0.830
151	very weak	0.807	0.807

3. Alloy 3 (55.8 at.% Ru)

Radiation	Cu Kα
Crystal Structure Determined	Face-centered orthorhombic
Lattice Parameters	a = 4.295 Å
	b = 4.192 Å
	c = 3.439 Å

hkl	intensity	'd' spacings, Å observed	calculated
001	very weak	very weak	3.439
111	very strong	2.247	2.260
200	strong	2.133	2.147
020	strong	2.088	2.095
002	medium strong	1.712	1.719
220	medium strong	1.495	1.499
202	medium strong	1.336	1.342
022	medium strong	1.327	1.329
311	medium strong	1.258	1.260
131	medium strong	1.238	1.239
222	strong	1.129	1.130
400	medium strong	1.070	1.073
420	medium strong	0.957	0.956
240	weak	0.936	0.941
402	medium strong	0.909	0.910
042	weak	0.896	0.895
313	medium strong	0.875	0.875
422	medium strong	0.834	0.835
242	medium strong	0.827	0.826
511	weak	0.817	0.817